

Distribution of genuine high-dimensional entanglement over 10.2 km of noisy metropolitan atmosphere

Lukas Bulla,^{1,2,*} Kristian Hjorth,^{1,3} Oskar Kohout,^{1,4,5} Jan Lang,¹ Sebastian Ecker^{1,2},^{1,2} Sebastian P. Neumann^{1,2},^{1,2} Julius Bittermann^{1,2},^{1,2} Robert Kindler^{1,2},^{1,2} Marcus Huber^{1,6,†} Martin Bohmann^{1,2,7,‡} Rupert Ursin,^{1,2,§} and Matej Pivoluska^{1,6,8,9,¶}

¹*Institute for Quantum Optics and Quantum Information, Austrian Academy of Sciences, Boltzmanngasse 3, 1090 Vienna, Austria*

²*Vienna Center for Quantum Science and Technology, Faculty of Physics, University of Vienna, Boltzmanngasse 5, 1090 Vienna, Austria*

³*Department of Physics, Faculty of Natural Sciences, Norwegian University of Science and Technology, NO-7491 Trondheim, Norway*

⁴*Fraunhofer Institute for Applied Optics and Precision Engineering IOF, Albert-Einstein-Strasse 7, 07745 Jena, Germany*

⁵*Friedrich-Schiller-Universität Jena, Fürstengraben 1, 07743 Jena, Germany*

⁶*Vienna Center for Quantum Science and Technology, Atominstytut, Technische Universität Wien, Stadionallee 2, 1020 Vienna, Austria*

⁷*Quantum Technology Laboratories GmbH—qtlabs, Clemens-Holzmeister-Straße 6/6, 1100 Vienna, Austria*

⁸*Institute of Computer Science, Masaryk University, 602 00 Brno, Czech Republic*

⁹*Institute of Physics, Slovak Academy of Sciences, 845 11 Bratislava, Slovakia*



(Received 13 January 2023; accepted 17 April 2023; published 30 May 2023)

Our study investigates the presence of high-dimensional entanglement in a recent demonstration of a noise-resistant quantum key distribution (QKD) protocol presented in [Phys. Rev. X **13**, 021001 (2023)]. We determined that it is possible to certify the dimensionality of the distributed entangled states to be at least three. To demonstrate this, we developed an energy-time entanglement discretization technique, as well as an improved witness for entanglement dimensionality. Our results provide insight into the complex relationship between high-dimensional entanglement and the noise resistance of QKD protocols operating in high dimensions.

DOI: [10.1103/PhysRevA.107.L050402](https://doi.org/10.1103/PhysRevA.107.L050402)

Introduction. Quantum entanglement [1,2] is arguably one of the most important phenomena in quantum physics. While in the early days of quantum mechanics, entanglement raised the controversial question of the completeness of the theory [3], today entanglement is revealed as an invaluable resource, enabling many important quantum communication protocols, such as quantum teleportation [4], superdense coding [5], and quantum key distribution (QKD) [6].

In many applied implementations of quantum communication protocols, photons entangled in the polarization degree of freedom are favored due to their simple and well-established way of manipulation and measurement. However, the process of spontaneous parametric down-conversion (SPDC), which is used to generate polarization entanglement, natively produces photons also entangled in other photonic degrees of freedom (DOFs); see, e.g., [7–9]. Recently, there has been an increased interest in building setups to control these DOFs [10–17] with the goal to access higher-dimensional Hilbert spaces. The possible advantages of higher-dimensional (qudit) over two-dimensional (qubit) photonic entanglement in quantum communication were already observed at the beginning of this century: qudit entanglement was shown to enable higher key rates and better noise resistance in QKD [18], higher

communication rates in superdense coding [19], and novel protocols like the quantum secret sharing [20]. While qudit-entangled states admit a higher amount of noise before losing their entanglement completely, it is a challenge to efficiently use this effect in experimental setups [21,22] and even more so to harness this noisy entanglement in communication protocols [23,24]. The reason for this is that, in experiments over very noisy channels, such as free-space communication [25], satellite to ground links [26], or underwater communication [27,28], the surviving entanglement between two qudits is restricted to qubit subspaces and thus not genuinely high-dimensionally entangled [21]. Indeed, genuine high-dimensional entanglement was certified before only for moderate distances, and additionally, the experiment required the use of two different DOFs simultaneously [29].

Recently, a high-dimensional QKD protocol was shown to yield a noise resilience advantage over a 10.2-km metropolitan horizontal free-space channel [30]. Curiously, increased noise resistance is not a proof of genuine high-dimensional entanglement by itself. Indeed, to experience increased noise resistance, one can imagine a situation where high-dimensional entanglement is created at the source, but the communicating parties at the end points can only certify entanglement in two-dimensional subspaces: this would be fully sufficient for QKD and the high-dimensional entanglement would therefore only serve as a resource to provide a noise-resistant distribution of qubit entanglement. This would, however, always limit the rate to be below one secret bit per photon pair. A recent experiment [30], indeed showed strictly less key rate per coincidence, yet exhibited significant noise advantages.

*lukas.bulla@oeaw.ac.at

†marcus.huber@tuwien.ac.at

‡martin.bohmann@qtlabs.at

§rupert.ursin@oeaw.ac.at

¶mpivoluska@mail.muni.cz

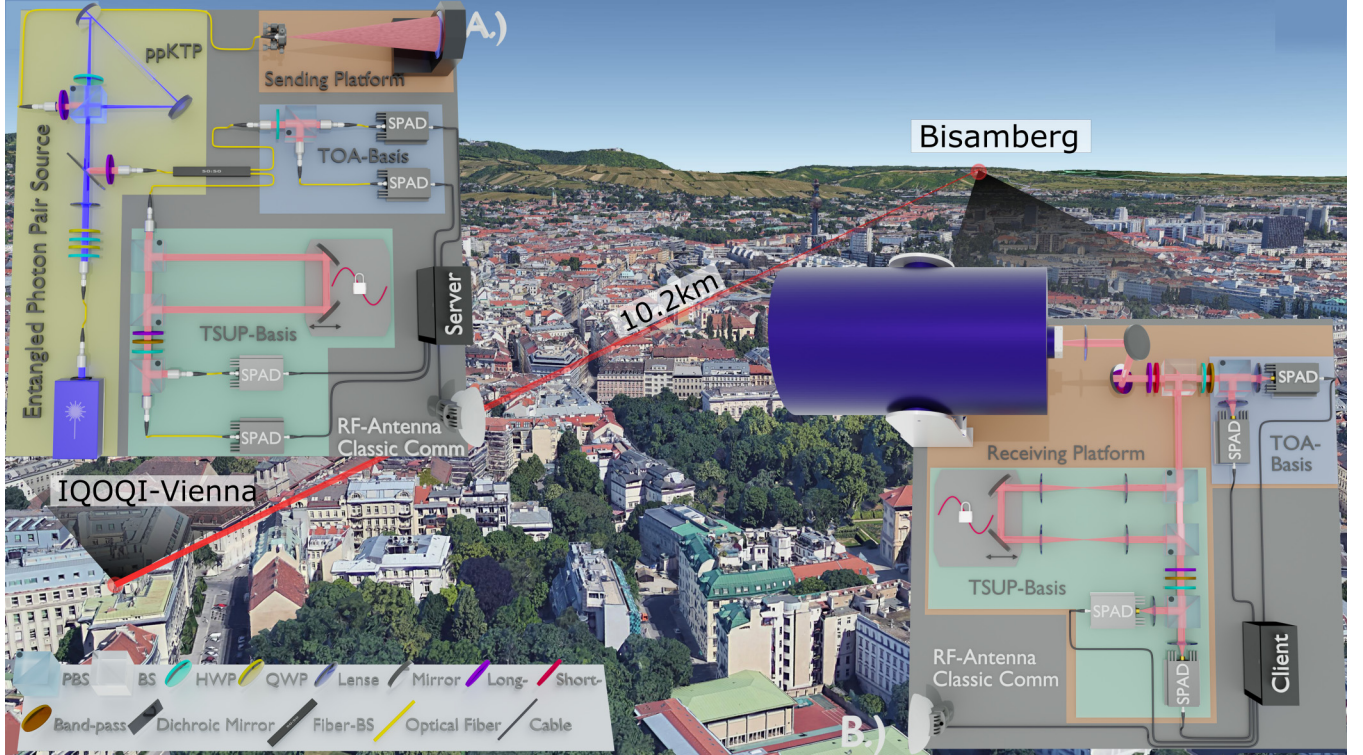


FIG. 1. (a) The setup at the IQOQI laboratory (Alice) with a hyperentangled photon pair source pumped by a ^{39}K stabilized Laser at 404.532 nm. The hyperentangled state was set by adjusting a combination of half-wave plate (HWP) and quarter-wave plates (QWP). The hyperentangled photons produced at 808.9 nm in a ppKTP crystal are separated and guided to Alice and Bob. A 50:50 beam splitter (BS), at Alice's receiver, randomly sends the incoming photons to either the basis measurement or the temporal superposition (TSUP) basis measurement. The Mach-Zehnder-Interferometer (MZI) in the TSUP basis uses Polarizing beam splitters followed by a measurement in the D/A-basis. The photon detection events are recorded by single-photon avalanche diodes (SPAD), time stamped by the time-tagging module and streamed to the server. (b) Receiver at the Bisamberg laboratory (Bob). The received photons are guided to the detection modules after filtering the background noise with filter combinations. Bob's setup is identical with that of Alice, with the difference of having two $4f$ systems in the MZI to compensate for the atmospheric turbulence and Bobs MZI is phase locked to a ^{87}Rb stabilized laser at 780.23 nm. Both MZI's together form a postselection-free Franson interferometer where each side is separated by 10.2 km.

A natural follow-up question for understanding the role of high-dimensional entanglement in this context is whether both sides actually share a genuinely high-dimensional entangled state after the noisy free-space channel is applied to the high-dimensional states. In this Letter we reanalyze the data from an alternative perspective and develop alternative methods for the certification of genuine high-dimensional time bin entanglement. As a result, we report the distribution of genuine three-dimensional entanglement in a single DOF over a 10.2-km metropolitan horizontal free-space channel.

Experimental setup. The experimental photon-pair state is created via SPDC by superposing wavelength-degenerate $\lambda_{\text{SPDC}} = 808.9\text{ nm}$ SPDC photons in a Sagnac interferometer. The SPDC photons are emitted by a type-II ppKTP crystal, which is bidirectionally pumped with a $\lambda_p = 404.453\text{ nm}$ continuous wave laser. The produced state is entangled simultaneously in the time energy and the polarization DOFs and can be described as

$$|\Psi\rangle_{AB} = \int dt f(t) |t, t\rangle \otimes (|H, H\rangle + e^{-i\phi} |V, V\rangle), \quad (1)$$

where $f(t)$ is a continuous function of time t , determined by the coherence time of the laser and $H(V)$ indicates the

horizontal (vertical) polarization state. The generated entangled photon pairs exit either side of the polarizing beam splitter of the Sagnac source; see Fig. 1. Then one photon is detected locally at Alice's laboratory where the source is located and the other one is guided to the sending platform and transmitted over a horizontal free-space channel to Bob's laboratory at 10.2-km distance. The sending platform consists of a Newtonian telescope with a mounted achromatic sending lens ($f = 257\text{ mm}$), where the telescope is used for tracking and the lens as a sending aperture. A Cassegrain telescope ($f = 2032\text{ mm}$) receives the photons at Bob's laboratory and guides them to the measurement setup.

Alice's and Bob's measurement setups consist of a time-of-arrival (TOA) and a time-superposition measurement (TSUP), each implementing measurement bases is described in the section titled "Discretization and certification." The TOA-basis measurement consists of a projective measurement in the Horizontal-Vertical (H-V)-basis and recording the photon arrival times in continuously streamed time tags. When processing these streams, one benefits from the hyperentangled state [10, 11] by taking polarization entanglement into account and passively sorting out photons not correlated in the polarization DOF, increasing the signal-to-noise ratio (SNR) in

the TOA basis. The TSUP basis uses an imbalanced Mach-Zehnder interferometer (MZI), with a path length difference of $\tau_{\text{MZI}} = 2.7 \text{ ns}$, to superpose the photons' long and short paths. The path difference τ_{MZI} supersedes the coherence time of the SPDC photons ($\tau_p \sim 3 \text{ ps}$), which is necessary to resolve the time of arrival of the detected photons. Alice's and Bob's local MZIs together form a Franson interferometer [31] to measure nonlocal two-photon interference. The local MZIs consist of two polarizing beam splitters, which map the polarization H-V to the short or long path. Using a diagonal or antidiagonal polarization (D-A) measurement after the MZIs, one deletes the which-path information and completes the Franson interferometer for nonlocal temporal interferometry. By using the hyperentangled state, we increase the efficiency of the Franson interferometer by mapping polarization to time-energy entanglement (see [29] for details). Additionally, we implement a $4f$ system (see [32] for details) in Bob's local MZI to compensate for the turbulent atmosphere. Furthermore, both MZIs and the source have to be phase stable with respect to each other, which is achieved by phase-locking them onto an atomic hyper-fine transition. Further details on the experiment can be found in [30], where we used the same free-space link to implement a noise-resistant high-dimensional QKD protocol.

Results. To certify three-dimensional entanglement, we first discretize the time-energy part of the produced continuous DOF state presented in Eq. (1) into a 4×4 -dimensional state $\rho_{\Delta t}$. This is achieved by coarse-graining the continuous time of arrival into time bins of variable length Δt (see "Discretization and certification" section for details and [21,30]). Then, for various choices Δt we lower-bound the fidelity of $\rho_{\Delta t}$ to the four-dimensional maximally entangled state $|\phi_4^+\rangle = \frac{1}{2} \sum_{i=0}^3 |ii\rangle$. Fidelity values larger than one-half certify the Schmidt number of $\rho_{\Delta t}$ (i.e., the smallest basis required to write down $\rho_{\Delta t}$) to be at least 3 [14] and thus it certifies $\rho_{\Delta t}$ to be at least genuinely three-dimensionally entangled.

The lower bounds on fidelity graphically presented in Fig. 2 are certified for 200 s blocks of discretized measurement data obtained at different points in time during the experiment. The results clearly show that the certified fidelity is higher for shorter time bins and the highest fidelity is observed at $\Delta t = 540 \text{ ps}$. This observation can be explained by the random distribution of accidental coincidence counts caused by external noise. In contrast, the signal coincidences caused by the entangled photons are always time-correlated in the time of arrival. Therefore, choosing shorter time bins in effect filters out more accidental counts. The minimal size of Δt is fundamentally limited by the coherence time of the SPDC photons τ_p . Further, feasible values of Δt are severely restricted by the electronic jitter of the detectors and the time-tagging modules. All of these effects decrease the precision of time-tagging. This kind of noise affects the certified fidelity more strongly for lower values of Δt . We indeed observe that for Δt below 540 ps the certified fidelity starts to rapidly decrease again.

Discretization and certification. The crucial component of TOA discretization is the coarse-graining of time-tagged detection event streams into time bins of length Δt . Subsequently, d time bins are collected into a time frame, which

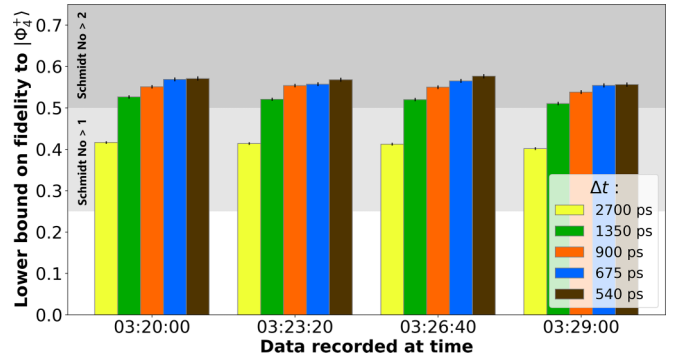


FIG. 2. Entanglement dimensionality witness. To certify entanglement dimensionality we use different discretisations with $d = 4$. For different time bin length (left to right) $\Delta t \in \{2700, 1350, 900, 675, 540\} \text{ ps}$, we evaluate the fidelity of the time-energy part of the discretised distributed state to maximally entangled state $|\phi_4^+\rangle = 1/\sqrt{4} \sum_{i=0}^3 |ii\rangle$. The integration time of all data points is 200 s and the fidelity is evaluated throughout the duration of the experiment. Fidelity strictly above 0.25 certifies that the underlying state has a Schmidt number of at least 2 and thus is entangled, while fidelity strictly above 0.5 certifies that the underlying state has a Schmidt number value of at least 3 and thus the correlations present in the state cannot be encoded using any qubit-entangled state.

determines the dimensionality $d \times d$ of the discretized Hilbert space. Conventionally, time frames are composed of d subsequent time bins (see, e.g., [21,30]). Applying this approach to our data does not lead to a certification of high-dimensional entanglement (see Fig. 2 with $\Delta t = 2700 \text{ ps}$). As explained above, shorter time frames effectively contain less accidental coincidences. In turn, to have shorter time frames it is instrumental to be able to decrease the time bin length Δt . For the

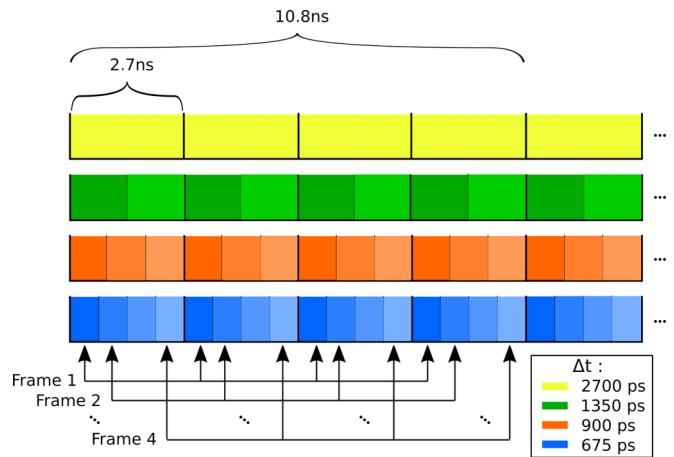


FIG. 3. Discretization we used to calculate the Schmidt number certificates. The time delay between interferometer arms is $\tau_{\text{MZI}} = 2.7 \text{ ns}$. Each measured time interval of length 10.8 ns is divided into time bins of size Δt . In the figure we used values (top to bottom) $\Delta t \in \{2700, 1350, 900, 675\} \text{ ps}$. Subsequently, time bins in the analyzed time interval with starting times exactly 2.7 ns apart are collected into a time frame. These were chosen specifically because we can use our measurement setup to measure projections onto some superpositions of bins with the same color.

conventional method this requirement translates to shortening the MZI delay τ_{MZI} on demand (see [13] for an experiment with variable τ_{MZI}) or the use multiple MZI interferometers. However, both methods are hard to implement for spatially separated interferometers.

To overcome this complication, we utilize an alternative coarse-graining scheme, which allows us to probe four-dimensional subspaces spanned by nonneighboring time bins of variable length Δt . Our method assigns four time bins with starting times exactly τ_{MZI} apart to a single time frame. If the time bin length Δt divides τ_{MZI} , such time frames can be interleaved so that an entire time-tagged measurement stream is covered (see Fig. 3). The main advantage of this method is that time bins probing four-dimensional subspaces can be much shorter than required by the conventional method. Such short time frames allow for a larger fraction of accidental clicks to be postselected away as single clicks.

Subsequently, we associate basis vectors $|0\rangle, |1\rangle, |2\rangle, |3\rangle$ to time bins in each time frame. The TOA measurement therefore corresponds to a projection onto the computational basis of the 4×4 Hilbert space defined by the time bin length Δt . The definition of the discretized TSUP measurement is a little more involved. The Franson interferometer implemented in the TSUP measurement modules can essentially be seen as implementing projections

onto superpositions of two time bins, the first starting at time t and the second one starting at time $t + \tau_{\text{MZI}}$. For the time frames we defined above this corresponds to projections onto six vectors: $\{\frac{1}{\sqrt{2}}(|0\rangle \pm |1\rangle), \frac{1}{\sqrt{2}}(|1\rangle \pm |2\rangle), \frac{1}{\sqrt{2}}(|2\rangle \pm |3\rangle)\}$. Clearly $\{\frac{1}{\sqrt{2}}(|0\rangle \pm |1\rangle), \frac{1}{\sqrt{2}}(|2\rangle \pm |3\rangle)\}$ form a complete four-dimensional Hilbert space basis and we will denote the projective measurement associated to this basis TSUP_1 . On the other hand, vectors $\frac{1}{\sqrt{2}}(|1\rangle \pm |2\rangle)$ need to be supplemented with another two orthogonal vectors from a subspace spanned by $|0\rangle$ and $|3\rangle$. We opted to approximate the measurement counts for projection onto this subspace with counts for projections onto $\{\frac{1}{\sqrt{2}}(|3\rangle \pm |0'\rangle)\}$, where $|0'\rangle$ is a time bin starting exactly τ_{MZI} after the start of time bin associated with $|3\rangle$. We denote the projective measurement associated to this second basis as TSUP_2 . Coincidence matrices for simultaneous measurements by both parties in these three bases can be obtained from the measurement data and postprocessed into outcome probabilities. These are subsequently used to obtain lower bounds for density matrix elements $\langle ii | \rho_{\Delta t} | ii \rangle$ for all $i \in \{0, 1, 2, 3\}$ and for $\text{Re}(\langle ii | \rho_{\Delta t} | i+1, i+1 \rangle) = \text{Re}(\langle i+1, i+1 | \rho_{\Delta t} | i, i \rangle)$ for $i \in \{0, 1, 2\}$. While the former is just a probability to obtain the i th outcome in Alice's and Bob's laboratory simultaneously, the latter can be obtained using the following calculation:

$$\begin{aligned} & \frac{(\langle i | + \langle i+1 |)_A \otimes (\langle i | + \langle i+1 |)_B \rho_{\Delta t} (|i\rangle + |i+1\rangle)_A \otimes (|i\rangle + |i+1\rangle)_B}{4} \\ & + \frac{(\langle i | - \langle i+1 |)_A \otimes (\langle i | - \langle i+1 |)_B \rho_{\Delta t} (|i\rangle - |i+1\rangle)_A \otimes (|i\rangle - |i+1\rangle)_B}{4} \\ & - \frac{(\langle i | - \langle i+1 |)_A \otimes (\langle i | + \langle i+1 |)_B \rho_{\Delta t} (|i\rangle - |i+1\rangle)_A \otimes (|i\rangle + |i+1\rangle)_B}{4} \\ & - \frac{(\langle i | + \langle i+1 |)_A \otimes (\langle i | - \langle i+1 |)_B \rho_{\Delta t} (|i\rangle + |i+1\rangle)_A \otimes (|i\rangle - |i+1\rangle)_B}{4} \\ & = 2\text{Re}[\langle i, i | \rho_{\Delta t} | i+1, i+1 \rangle] + 2\text{Re}[\langle i, i+1 | \rho_{\Delta t} | i+1, i \rangle]. \end{aligned} \quad (2)$$

To obtain a lower bound on $2\text{Re}[\langle i, i | \rho_{\Delta t} | i+1, i+1 \rangle]$ it remains to derive an upper bound on the term $2\text{Re}[\langle i, i+1 | \rho_{\Delta t} | i+1, i \rangle]$. This can be done as follows. First, note that the real part of a complex number is always smaller than its absolute value, therefore

$$\begin{aligned} & 2\text{Re}[\langle i, i+1 | \rho_{\Delta t} | i+1, i \rangle] \\ & \leq 2|\langle i, i+1 | \rho_{\Delta t} | i+1, i \rangle| \\ & \leq 2\sqrt{\langle i, i+1 | \rho_{\Delta t} | i, i+1 \rangle \langle i+1, i | \rho_{\Delta t} | i+1, i \rangle}, \end{aligned} \quad (3)$$

where the last inequality is an application of the Cauchy-Schwartz inequality

$$|\langle ij | \rho | kl \rangle| \leq \sqrt{\langle ij | \rho | ij \rangle \langle kl | \rho | kl \rangle}.$$

Note that the fidelity of $\rho_{\Delta t}$ to $|\phi_4^+\rangle$ is defined as

$$F(\rho_{\Delta t}, |\phi_4^+\rangle \langle \phi_4^+|) = \frac{1}{4} \sum_{i,j=0}^3 \text{Re}(\langle ii | \rho_{\Delta t} | jj \rangle), \quad (4)$$

and thus it remains to lower-bound the six remaining real parts of density matrix elements $\text{Re}(\langle ii | \rho_{\Delta t} | jj \rangle)$, with $|i-j| > 1$.

This can be done using density matrix completion techniques based on the Sylvester's criterion [12,13], from which it follows that every subdeterminant of a positive-semi-definite matrix should be nonnegative. Performing these calculations on our experimental data leads to fidelity lower bounds which are presented in Fig. 2.

Discussion. In this Letter we revisited a recent experiment, where high-dimensional QKD experiment was performed over a long-distance free-space channel to successfully show an advantage in noise resistance. We shined more light on the role high-dimensional entanglement has played in this experiment. In particular, it was not clear whether the genuine high-dimensional entanglement created at the source actually survived the transmission over a very noisy atmospheric channel. Here we answered this question affirmatively. This was possible only thanks to developing an alternative way of looking at time bin entanglement, by relaxing the requirement that a time frame is composed of chronologically subsequent time bins. Indeed with the alternative technique we were able to use much shorter time bins for supreme noise

filtering and thus reported an experimental realization of high-dimensional entanglement distribution over a long-distance horizontal free-space channel.

We also believe that the techniques developed within our research can be further improved on, which would allow us to certify even higher-dimensional entanglement in the time-energy DOF. The simplest and most immediate upgrade to the setup would be adding another measurement setting to the Franson interferometer setup, which should allow us to add phase to the photon passing through the long arm and thus be able to measure projections on $\frac{|k\rangle \pm i|k+1\rangle}{\sqrt{2}}$. This would in effect improve our estimation of the first off-diagonal density matrix element [Eq. (2)] so that the estimation performed in Eq. (3) would not be needed. The second experimental improvement is more involved and consists of adding a capability to modify the MZI delay τ_{MZI} . Already measurements with two different values of τ_{MZI} as in [13] would allow efficient estimation of a larger number of density matrix elements of the experimental

state. This would allow more stringent constraints for the semi-definite programs used to complete the density matrix in the last step of the analysis, thus increasing the tightness of our bound.

Acknowledgments. M.P. acknowledges funding from Grant Agency of Masaryk University (GAMU) Project No. MUNI/G/1596/2019 and VEGA Project No. 2/0136/19. M.H. would like to acknowledge funding from the European Research Council (Consolidator Grant Cocoquest No. 101043705). M.P. and M.H. acknowledge funding from European Commission (Grant “Hyperspace” No. 101070168). L.B. acknowledges European Unions Horizon 2020 program Grant No. 857156 (OpenQKD) and the Austrian Academy of Sciences in cooperation with the FhG ICON-Programm Integrated Photonic Solutions for Quantum Technologies (InteQuant). L.B. also gratefully acknowledges financial support from the Austrian Research Promotion Agency (FFG) Agentur für Luft-und Raumfahrt (FFG-ALR Contracts No. 844360 and No. 854022).

- [1] R. Horodecki, P. Horodecki, M. Horodecki, and K. Horodecki, *Rev. Mod. Phys.* **81**, 865 (2009).
- [2] N. Friis, G. Vitagliano, M. Malik, and M. Huber, *Nat. Rev. Phys.* **1**, 72 (2019).
- [3] A. Einstein, B. Podolsky, and N. Rosen, *Phys. Rev.* **47**, 777 (1935).
- [4] C. H. Bennett, G. Brassard, C. Crépeau, R. Jozsa, A. Peres, and W. K. Wootters, *Phys. Rev. Lett.* **70**, 1895 (1993).
- [5] C. H. Bennett and S. J. Wiesner, *Phys. Rev. Lett.* **69**, 2881 (1992).
- [6] A. K. Ekert, *Phys. Rev. Lett.* **67**, 661 (1991).
- [7] R. W. Boyd, *Nonlinear Optics, Third Edition*, 3rd ed. (Academic, New York, 2008).
- [8] M. Erhard, M. Krenn, and A. Zeilinger, *Nat. Rev. Phys.* **2**, 365 (2020).
- [9] A. Anwar, C. Perumangatt, F. Steinlechner, T. Jennewein, and A. Ling, *Rev. Sci. Instrum.* **92**, 041101 (2021).
- [10] P. G. Kwiat, *J. Mod. Opt.* **44**, 2173 (1997).
- [11] J. T. Barreiro, N. K. Langford, N. A. Peters, and P. G. Kwiat, *Phys. Rev. Lett.* **95**, 260501 (2005).
- [12] A. Tiranov, S. Designolle, E. Z. Cruzeiro, J. Lavoie, N. Brunner, M. Afzelius, M. Huber, and N. Gisin, *Phys. Rev. A* **96**, 040303(R) (2017).
- [13] A. Martin, T. Guerreiro, A. Tiranov, S. Designolle, F. Fröwis, N. Brunner, M. Huber, and N. Gisin, *Phys. Rev. Lett.* **118**, 110501 (2017).
- [14] J. Bavaresco, N. Herrera Valencia, C. Klöckl, M. Pivoluska, P. Erker, N. Friis, M. Malik, and M. Huber, *Nat. Phys.* **14**, 1032 (2018).
- [15] N. Herrera Valencia, V. Srivastav, M. Pivoluska, M. Huber, N. Friis, W. McCutcheon, and M. Malik, *Quantum* **4**, 376 (2020).
- [16] E. A. Ortega, K. Dovzhik, J. Fuenzalida, S. Wengerowsky, J. C. Alvarado-Zacarias, R. F. Shiozaki, R. Amezcu-Correa, M. Bohmann, and R. Ursin, *PRX Quantum* **2**, 040356 (2021).
- [17] L. Achatz, L. Bulla, E. A. Ortega, M. Bartokos, J. C. Alvarado-Zacarias, R. Amezcu-Correa, M. Bohmann, R. Ursin, and M. Huber, Simultaneous transmission of hyper-entanglement in three degrees of freedom through a multicore fiber, *NPJ Quantum Inf.* **9**, 45 (2023).
- [18] D. Cozzolino, B. Da Lio, D. Bacco, and L. K. Oxenløwe, *Adv. Quantum Technol.* **2**, 1900038 (2019).
- [19] R. Cleve, D. Gottesman, and H.-K. Lo, *Phys. Rev. Lett.* **83**, 648 (1999).
- [20] X. S. Liu, G. L. Long, D. M. Tong, and F. Li, *Phys. Rev. A* **65**, 022304 (2002).
- [21] S. Ecker, F. Bouchard, L. Bulla, F. Brandt, O. Kohout, F. Steinlechner, R. Fickler, M. Malik, Y. Guryanova, R. Ursin *et al.*, *Phys. Rev. X* **9**, 041042 (2019).
- [22] X.-M. Hu, W.-B. Xing, B.-H. Liu, Y.-F. Huang, C.-F. Li, G.-C. Guo, P. Erker, and M. Huber, *Phys. Rev. Lett.* **125**, 090503 (2020).
- [23] M. Doda, M. Huber, G. Murta, M. Pivoluska, M. Plesch, and C. Vlachou, *Phys. Rev. Appl.* **15**, 034003 (2021).
- [24] X.-M. Hu, C. Zhang, Y. Guo, F.-X. Wang, W.-B. Xing, C.-X. Huang, B.-H. Liu, Y.-F. Huang, C.-F. Li, G.-C. Guo, X. Gao, M. Pivoluska, and M. Huber, *Phys. Rev. Lett.* **127**, 110505 (2021).
- [25] R. Ursin, F. Tiefenbacher, T. Schmitt-Manderbach, H. Weier, T. Scheidl, M. Lindenthal, B. Blauensteiner, T. Jennewein, J. Perdigues, P. Trojek *et al.*, *Nat. Phys.* **3**, 481 (2007).
- [26] S.-K. Liao, W.-Q. Cai, W.-Y. Liu, L. Zhang, Y. Li, J.-G. Ren, J. Yin, Q. Shen, Y. Cao, Z.-P. Li *et al.*, *Nature (London)* **549**, 43 (2017).
- [27] Z. Feng, S. Li, and Z. Xu, *Opt. Express* **29**, 8725 (2021).
- [28] F. Hufnagel, A. Sit, F. Bouchard, Y. Zhang, D. England, K. Heshami, B. J. Sussman, and E. Karimi, Investigation of underwater quantum channels in a 30 meter flume tank using structured photons, *New J. Phys.* **22**, 093074 (2020).
- [29] F. Steinlechner, S. Ecker, M. Fink, B. Liu, J. Bavaresco, M. Huber, T. Scheidl, and R. Ursin, *Nat. Commun.* **8**, 15971 (2017).
- [30] L. Bulla, M. Pivoluska, K. Hjorth, O. Kohout, J. Lang, S. Ecker, S. P. Neumann, J. Bittermann, R. Kindler, M. Huber, M. Bohmann, and R. Ursin, Non-local temporal interferometry for highly resilient free-space quantum communication, *Phys. Rev. X* **13**, 021001 (2023).
- [31] J. D. Franson, *Phys. Rev. Lett.* **62**, 2205 (1989).
- [32] J. Jin, S. Agne, J.-P. Bourgoin, Y. Zhang, N. Lütkenhaus, and T. Jennewein, *Phys. Rev. A* **97**, 043847 (2018).